Magnetic relaxation in the nanoscale granular alloy $Fe_{20}Cu_{20}Ag_{60}$

D. H. Ucko and Q. A. Pankhurst*
Department of Physics & Astronomy, University College London, Gower Street, London WC1E 6BT, United Kingdom

L. Fernández Barquín and J. Rodríguez Fernández
Departamento CITIMAC, Facultad Ciencias, Universidad de Cantabria, Santander 39005, Spain

S. F. J. Cox
ISIS Facility, Rutherford Appleton Laboratory, Chilton, Didcot OX11 0QX, United Kingdom

(Received 31 May 2000; published 23 August 2001)

The structural and magnetic properties of a representative member of a class of technologically relevant ternary metallic alloys have been studied in detail. The alloy, of composition $Fe_{20}Cu_{20}Ag_{60}$, is a member of the family of nanoscale granular alloys that are of current interest in both giant magnetoresistive alloys and nanocrystalline soft magnets. Samples were produced by mechanical alloying (70 h, argon sealed) and were homogeneous according to scanning electron microscopy and electron microprobe analysis. Room-temperature magnetoresistance measurements in applied fields up to $H=90$ kOe gave a value of 5% (at 90 kOe) for the $[R(H)-R(0)]/R(0)$ ratio. Rietveld calculations on high-resolution image plate data using a synchrotron source ($\lambda=0.6920$ Å) showed that the specimen comprised a dispersion of bcc $Fe_{60}Cu_{40}$ ($Im\text{-}3m$, $a=2.951$ Å) particles of mean size 5.5 nm in an fcc $Ag_{90}Cu_{10}$ ($Fm\text{-}3m$, $a=4.057$ Å) matrix. This structure was stable up to 380 K as revealed by differential scanning calorimetry. dc magnetization (peaks in zero-field-cooled data) and frequency-dependent ac susceptibility (in external dc magnetic fields from zero to 500 Oe) measurements showed blocking transitions between 280 and 300 K, with the onset of superparamagnetic behavior at higher temperatures. The superparamagnetic regime was confirmed at room temperature by the observation of anhysteretic $M(H)$ curves, and through zero field and applied field Mössbauer experiments in which a combined singlet plus doublet spectrum was transformed to a magnetically split sextet on application of an 11-kOe field. In all cases the blocking transitions were clearly affected by the existence of intergranular interactions, which shifted them to higher temperatures than would be expected from noninteracting grains. Evidence of intergranular interactions were also found in the dynamic behavior of the ac susceptibility data (small frequency-dependent shifts in the blocking temperature, Vogel-Fulcher activation processes). Muon spectroscopy was found to provide excellent corroborating information on the blocking transition, with a clear peak being found in the exponential decay rates of the depolarization spectra. The result establishes the feasibility of using muon spin relaxation to probe other superparamagnetic materials, with the advantage that measurements can be conducted in absolutely zero field.

DOI: 10.1103/PhysRevB.64.104433 PACS number(s): 72.15.Gd, 75.40.Gb

I. INTRODUCTION

Nanoscale Fe-based magnetic alloys comprising very fine magnetic grains embedded in a nonmagnetic metallic host are of interest from both applied and fundamental viewpoints.[1,2] Recent technological examples include nanocrystalline alloys for soft magnetic applications, and granular alloys for magnetoresistive applications. The former are obtained by controlled annealing of amorphous precursors such as Fe-Nb-Cu-Si-B and Fe-Zr-B-Cu.[3,4] Their outstanding soft magnetic properties are related to the growth of nanometre scale Fe-Si and α-Fe grains embedded in the amorphous matrix.[5–11] The latter include the binary Fe-Cu and Fe-Ag systems[12–16] and the ternary Fe-Cu-Ag and Fe-Co-Ag systems,[17–19] prepared by a variety of methods including sputtering, co-evaporation, ion implantation, melt spinning, sol-gel synthesis, and mechanical alloying. They show giant magnetoresistance (GMR) due to the formation of highly dispersed nanometre scale structures of magnetic grains in a nonmagnetic matrix, and the resultant high volume density of interfacial scattering sites.

At a fundamental level, the functional properties of these materials are intimately related to relaxation effects such as the onset of superparamagnetism. In the superparamagnetic state the atomic moments in a single-domain grain cooperatively undergo spontaneous thermally activated reversals in direction. Superparamagnetism is generally observed in those materials that exhibit GMR,[12–18] and has been nominated as the cause of GMR in some granular systems.[20] However, present studies of the role of superparamagnetism in granular alloys have focused on simplified model systems rather than more complex, but technologically relevant, systems. For example, there have been studies of superparamagnetism in nearly monodisperse ensembles of α-Fe particle deposited on nonmetallic supports, such as carbon,[21,22] MgO,[23] and Faujasite-type zeolites.[24] Meanwhile, studies to date on granular GMR alloys[25–28] have revealed complexities with regard to their fine-grained structural and magnetic characters, which have been an obstacle to analysis of their magnetic relaxation properties.

In an effort to advance our understanding of the more complex granular systems, we have in this work undertaken

a comprehensive study of relaxation effects in a technologically relevant Fe-based granular alloy. A key to our approach is the use of several different experimental techniques on a single sample, to obtain relaxation data over a wide range of measurement time scales. This study is conducted on a ''nonideal'' material, where the challenges relating to the effects of grain-size distributions and intergranular magnetic interactions are a raison d'être for the work, rather than an inconvenience or a hindrance.

In recent work we surveyed the magnetic and structural properties of the ternary alloy system Fe-Cu-Ag as prepared by high-energy mechanical alloying.[29,30] We found that in some cases mechanical alloying produced materials with nanoscale structures. In binary Fe-Ag alloys the milling product comprised bcc α-Fe grains dispersed in an fcc Ag matrix, with little or no mixing between the two metals, and mean grain sizes of order 6–10 nm depending on composition.[29] Even finer structures were observed when Cu was incorporated into the system. Indeed, in equimolar Fe-Cu-Ag the resultant structure was on such a fine scale that the product could be considered to be amorphous.[29] For small concentrations of Cu a solid solution was formed with the α-Fe grains, so that the resultant microstructure comprised bcc Fe-Cu grains in an fcc Ag matrix.[29]

For the purpose of the present investigation we have focused on an alloy of composition $Fe_{20}Cu_{20}Ag_{60}$. This was selected as it gave rise to a finer grain size than was achievable in a binary Fe-Ag alloy, while the magnetic properties of the bcc Fe grains were found to be largely unaffected by the incorporation of Cu.[29] Moreover, the values for the magnetoresistance $R(H)$ at 300 K lie around $[R(H)-R(0)]/R(0)=3-5\%$ between zero and 90 kOe in this compositional area of the ternary Fe-Cu-Ag phase diagram, which compares well with other granular systems.[31] Our aim was to characterize the magnetic relaxation in the system, and to establish the nature of any relaxation effects that might be present. To do this we applied a number of standard methods for probing magnetic relaxation in nanoscale systems: temperature-dependent magnetic hysteresis, zero-field-cooled–field-cooled dc magnetometry, frequency-dependent ac susceptibility, and Mössbauer spectroscopy. These methods allowed us access to data on measurement time scales ranging from $\sim 10^{-9}$ to 10^{2} s.

In addition to this we applied the technique of muon spin relaxation (μSR) to the problem. This is an uncommon approach to studies of superparamagnetism, with the only reports to date dealing with the iron storage protein ferritin,[32] a dilute alloy of 2 at.% Co in Cu,[33,34] and a dilute dispersion of 0.1 vol% Fe in an Ag thin film.[35–37] There are some especially advantageous features of μSR for the Fe-Cu-Ag system, notably that the data obtained are selectively sensitive to the relaxing moments in the sample, and that the measurement time scales fall in a region of interest close to those afforded by Mössbauer spectroscopy and by ac susceptibility.

In the following, Sec. II covers the experimental techniques used, Sec. III deals with the sample preparation method and magnetoresistive and structural characterization, and Sec. IV comprises the magnetic characterization results, covering a wide range of time scales, including data analysis. The results are drawn together and discussed, and the role of magnetic interactions in the observed relaxation is appraised, in Sec. V.

II. EXPERIMENTAL DETAILS

Samples were prepared from >99.9% pure elemental Fe and Ag powders (Aldrich Chemical Co.) and elemental Cu powder (Strem Chemicals Inc.), used as supplied. Mechanical alloying was carried out using a Fritsch Pulverisette 7 high-energy planetary ball mill, with hardened steel bowls and balls (type 4301 stainless steel: 68 at.% Fe, 19 at.% Cr, 8 at.% Ni, 2 at.% Mn, 2 at.% Si and traces of S and C) operating at a rotation frequency of 600 rpm. Approximately 7 g of sample was used, with a ball to powder mass ratio of 12 to 1. To prevent excessive heating the mill was operated for 2-h periods, interspersed with cooling down periods of 1 h, which kept the mean temperature of the bowls and balls at 40 ± 5 °C. The samples were milled for 70 h to ensure completion of the alloying process. The milling bowls were sealed in argon and tightly clamped to prevent oxidation.

Sample morphology, composition, and homogeneity was tested via scanning electron microscopy and energy dispersive x-ray analysis (EDAX) on a Hitachi S-4000 and on a Jeol EMA. Measurements were made using a 1-μm beam spot size. Specimens were prepared by loading the sample powder into an epoxy resin plug, and polishing the plug surface with increasingly fine standard abrasive paper.

Magnetoresistance measurements were carried out on compacted samples inserted into a Quantum Design multipurpose instrument. The standard four-probe geometry was adopted. An external dc Keithley 220 power supply (20 mA) was used, and voltages were recorded using an HP 34420A nanovoltmeter.

Structural analysis was carried out via high resolution x-ray diffraction using the synchrotron radiation source at the Daresbury Laboratory, UK. A curved image plate detector was used, on Station 9.1, and the source radiation was tuned to a wavelength of 0.6920 Å, avoiding fluorescence in the sample. The data were analyzed by standard Rietveld refinement using the FULLPROF program as supplied by the Laboratoire Leon Brillouin, Saclay.[38,39]

Differential scanning calorimetry (DSC) measurements were made with a Shimadzu DSC-50 calibrated against In and Zn standards, at a heating rate of 20 K min^{-1}. Samples were placed in open platinum pans in an atmosphere of flowing nitrogen that reduced, but did not eliminate completely, the likelihood of oxidation.

^{57}Fe Mössbauer spectra were collected in the range 80–300 K with a Wissel MA-260S constant acceleration spectrometer and a liquid-nitrogen cryostat. A triangular drive wave form was used, and the spectra were folded to remove baseline curvature. Calibration was made with respect to α iron at room temperature. The spectra were analyzed using a least-squares fitting program based on combinations of Lorentzian sextets and doublets for the subspectra of magnetically ordered crystalline or paramagnetic phases, respectively.

Field-dependent magnetization curves (*M-H* curves) were

recorded at room temperature in applied fields up to 5 kOe using an Aerosonic 3001 vibrating sample magnetometer. dc magnetization (M_{dc}) data were recorded in external fields of up to 30 kOe using a Quantum Design MPMS superconducting quantum interference device (SQUID) magnetometer operated under zero-field-cooled and field-cooled sequences. ac susceptibility (χ_{ac}) measurements were made using a Quantum Design PPMS. Data were recorded from 5 to 350 K with a sinusoidal excitation field of amplitude 10 Oe oscillating at frequencies from 30 Hz to 10 kHz. Both in-phase and out-of-phase data were recorded at a fixed frequency while the sample temperature was increased at ~0.1 K min around the transitions, and at 0.3 K min^{-1} in other temperature regions. External biasing fields of $H_{dc}=500$ and 1000 Oe were applied for some specific cases.

μSR experiments were performed on the ARGUS and MuSR spectrometers at the ISIS pulsed neutron and muon facility at the Rutherford Appleton Laboratory, UK. Measurements were made in zero field and in longitudinal fields of up to 2 kOe, at temperatures ranging from 10 to 340 K. The powder samples were sealed in a 1.5×1.5-cm^2 silver foil package attached to a pure silver mounting plate. High quality spectra (up to 50 million counts per run) were collected. These were analyzed over the time range $t\leqslant15\,\mu$s using the WiMDA computer program.[40]

III. SAMPLE PREPARATION AND MAGNETORESISTIVE AND STRUCTURAL CHARACTERIZATION

Mechanically alloyed samples were prepared by high-energy ball milling a mixture of iron, copper and silver powders with initial composition $Fe_{20}Cu_{20}Ag_{60}$. The product after 70 h of milling was a fine powder, mid gray in color, with no sign of the clumping that would be expected if the grains had bulk magnetic moments. Scanning electron microscope (SEM) micrographs showed that the product was comprised of irregularly shaped grains with sizes ranging from approximately 10 to 60 μm. EDAX analysis gave a measure of the overall atomic percentages of those elements heavier than oxygen. The sample that we focus on here had a composition $Fe_{20.2}Cu_{19.1}Ag_{60.7}$, with an accuracy of order ±1.0 at.% on Fe and Ag, and ±0.5 at.% on Cu. Traces of Cr impurities were noted, at the level of 0.1–0.2 at.% Cr, indicating a minor contamination from the stainless-steel milling containers. The slightly enhanced Fe content is also attributable to material from the milling balls and containers. SEM/EDAX elemental area scans (Fe, Cu, and Ag) showed that the sample was entirely homogeneous at the micron scale level of instrumental resolution.

The magnetoresistance behavior $R(H)$ of the sample after compaction is shown in Fig. 1 for fields of up to $H=90$ kOe at 300 K. It shows a sharp initial drop in $R(H)$ which progressively tends to saturate at higher fields. The magnetoresistance ratio $[R(H)-R(0)]/R(0)$ reaches around 5% at the highest field. This behavior is similar to other mechanical alloys of Fe-Cu-Ag (Ref. 31) and Fe-Co-Ag (Ref. 19) and establishes the GMR character of this alloy.

X-ray-diffraction data for the sample are shown in Fig. 2.

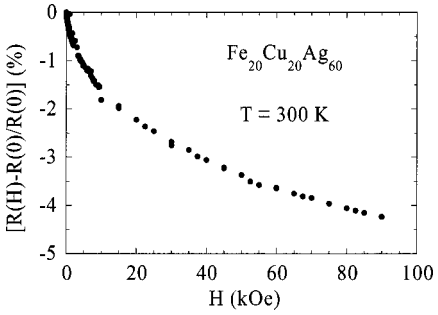

FIG. 1. Field-dependent magnetoresistance in an $Fe_{20}Cu_{20}Ag_{60}$ granular alloy at 300 K, measured using the standard four-probe geometry and dc currents.

Referring to earlier structural studies of Fe-Cu-Ag,[29] we note that the pattern is similar to that of ball milled silver: an fcc pattern with broad lines. Estimates of the lattice parameter from this pattern give $a\approx4.05$ Å, which is lower than that of pure Ag ($a\approx4.07$ Å). Since it is known[29] that even small amounts of Cu alloyed with Ag results in a significant reduction in the lattice parameter ($a\approx4.00$ Å for $Cu_{20}Ag_{80}$), this indicates that some Cu (of order 10 at.%, see below) is incorporated into the Ag lattice. There is no sign of the fcc pattern of pure Cu, which has $a\approx3.62$ Å and has lines at lower angles than those of pure Ag. Given that Fe and Ag do not alloy as readily as Cu and Ag,[29] we surmise that the majority of the Cu may be alloyed with the Fe (in a ratio of order 40 at.% Cu to 60 at.% Fe, see below), and that together they are separated from the Ag-rich Ag-Cu grains. In keeping with this, the second fcc (Ag-rich Ag-Cu) peak near 19°, which overlaps with the first bcc (Fe-Cu) peak, is broader than would be expected for the fcc phase alone, given the widths of the other fcc peaks. This is consistent with the 19° peak deriving from a combination of fcc and bcc phase peaks.

Given the coincidence of the fcc and bcc peaks along the rest of the diffraction pattern, it is not trivial to separate the contributions from the two phases. Nevertheless, we have

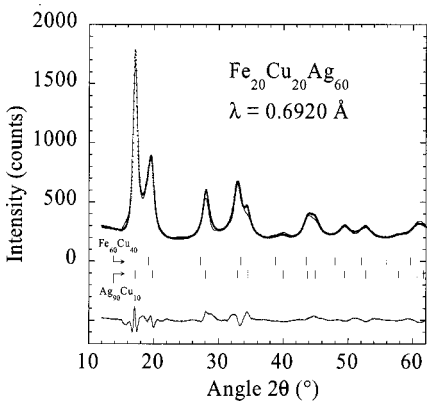

FIG. 2. X-ray-diffraction pattern of an $Fe_{20}Cu_{20}Ag_{60}$ granular alloy recorded on a synchrotron source of wavelength $\lambda=0.6920$ Å. The solid line is a Rietveld fit of the data using a model of bcc $Fe_{60}Cu_{40}$ grains supported in an fcc $Ag_{30}Cu_{10}$ matrix. The bottom trace is the difference between the fit and the data.

TABLE I. Crystallographic data for a ball milled $Fe_{20}Cu_{20}Ag_{60}$ granular alloy as determined by Rietveld analysis of x-ray data collected on a synchrotron radiation source of wavelength $\lambda = 0.6920$ Å. Two main phases were refined, an fcc Ag-Cu and a bcc Fe-Cu substitutional alloy, plus a minority amorphous component that accounted for ~1.7 wt % of the sample. Crystallite sizes and strains were obtained via a standard procedure,[42–44] using linewidth data from all the observed peaks.

Phase	Lattice parameter (Å)	Crystallite size (Å)	Strain (%)	Bragg R factor (%)	Relative amount (wt %)
$Fe_{60}Cu_{40}$	2.951 ± 0.002	55 ± 5	8.0 ± 0.5	8.6	27.1
$Ag_{90}Cu_{10}$	4.057 ± 0.001	43 ± 5	5.5 ± 0.5	10.9	72.9

been able to derive a Rietveld refinement of the pattern, using pseudo-Voigtian profiles, and modeling a pattern which included a superposition of diffraction peaks due to fcc Ag-Cu and bcc Fe-Cu grains. The high statistical quality of the pattern allowed the atomic compositions of the two phases to be included as fitting parameters. The best fit obtained had a good quality-of-fit Bragg factor of $R_B \leqslant 11\%$. This fit is shown in Fig. 2, and derived parameters are given in Table I. The fcc phase was fitted as $Ag_{90}Cu_{10}$, and the bcc phase was fitted as $Fe_{60}Cu_{40}$, so that the alloy may be regarded as

$$Fe_{20}Cu_{20}Ag_{60} = (Fe_{20}Cu_{13.33})_{\text{dispersed}}(Ag_{60}Cu_{6.67})_{\text{matrix}}.$$

The Rietveld parameters are in agreement with the postulated phases, although the weighting contribution of the Fe-Cu phase is a little more than expected given the $Fe_{20}Cu_{20}Ag_{60}$ composition (27.1 wt % compared to the expected 25.4 wt %). This may be due to the presence of a small pseudoamorphous contribution, associated with ~1–2 wt % of the sample, which was included in the fit. Such a contribution is most likely attributable to disordered grain boundaries.[41]

The Rietveld refinement allows us to distinguish between the line-broadening effects due to grain size and strain. Mean values for the sizes and strains of the $Fe_{60}Cu_{40}$ and $Ag_{90}Cu_{10}$ phases (Table I) were obtained via a standard procedure,[42–44] using the linewidth data from all the observed peaks. The sizes and strains are close to those found in other mechanically alloyed systems.[43,45,46]

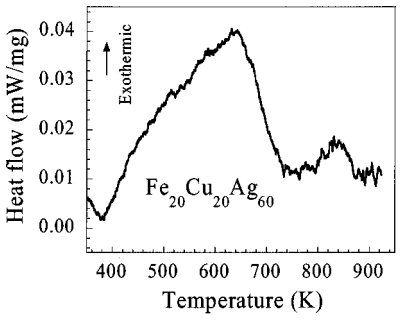

FIG. 3. Differential scanning calorimetry curve for an $Fe_{20}Cu_{20}Ag_{60}$ granular alloy. The broad asymmetric peak with a maximum at 640 K is associated with lattice recovery and the decomposition of the Fe-Cu and Ag-Cu grains into separate Fe, Cu, and Ag. The peak at 840 K is associated with the recrystallization of the Fe, Cu, and Ag grains.

A DSC scan for the sample is shown in Fig. 3. The small signal magnitude, of order 0.04 mW/mg, is typical of a Ag-rich material which does not readily support strain energy. Pure Ag when milled has a virtually flat DSC trace, with a magnitude of less than 0.01 mW/mg.[30] The main broad exothermic peak, with its maximum near 640 K, is reminiscent of the largest exotherm in ball milled $Fe_{50}Cu_{50}$ at 650 K.[30] The position of the smaller exothermic peak at 840 K is close to that of the largest peak seen in ball milled $Fe_{50}Ag_{50}$ at 800 K.[30] Drawing from the previous study, we associate the broad exotherm maximum at 640 K with the energy release due to lattice recovery and decomposition of the Fe-Cu grains into separate Fe and Cu metals, and the peak at 840 K with the recrystallization of the Fe, Cu, and Ag grains. We also note that the exothermic response begins at a relatively low temperature, 380 K, which imposes a rather strict experimental limitation on the temperatures to which the sample may be heated without incurring structural rearrangement.

On the basis of the foregoing experiments we conclude that the sample comprises nanoscale grains of a bcc $Fe_{60}Cu_{40}$ alloy interspersed between nanoscale grains of fcc $Ag_{90}Cu_{10}$. The mean sizes of these grains, determined from the x-ray data, are of order 5 and 4 nm for the Fe-Cu and Ag-Cu, respectively. We note that the milling route to the formation of the system is likely to result in a relatively broad distribution of grain sizes. We also note that the magnetic grains are sufficiently small that we may reasonably expect that rapid relaxation effects, including the presence of a superparamagnetic regime, might be observed.[47] It is also true that this is a relatively concentrated magnetic system and hence we may expect that intergranular magnetic interactions will be present.[10,47]

IV. MAGNETIC CHARACTERIZATION

A. Experimental studies of superparamagnetism

Superparamagnetic relaxation was considered by Néel[48] and later by Brown[49] for the case of a monodisperse ensemble of noninteracting particles or grains. Both derived an activation law for the relaxation time τ of the magnetization of the form

$$\tau = \tau_0 \exp(\Delta E / k_B T), \tag{1}$$

where ΔE is the energy barrier to a moment reversal, and k_BT is the thermal energy. In the case of uniaxial anisotropy, $\Delta E = KV$, where K is the anisotropy energy density and V is the particle or grain volume. Brown predicted that the pre-exponential factor τ_0 should be of order 10^{-10}–10^{-12} s and only weakly dependent on temperature.[49] The influence of interparticle or intergranular interactions on superparamagnetic relaxation has subsequently been the subject of a number of experimental and theoretical studies.[47,50–53] In the case of dipolar interactions it has been suggested that the modified relaxation time retains the form of Eq. (1), with an increased energy barrier ΔE, and a smaller pre-exponential factor, in the range 10^{-17}–10^{-18} s.[47]

In any observation of superparamagnetic relaxation one is constrained to measuring the relaxation time τ with respect to the measuring time τ_m of the specific experimental technique being used. If $\tau \ll \tau_m$ the relaxation is so fast relative to the experimental time window that the ensemble behaves as if it were paramagnetic. If $\tau \gg \tau_m$ the relaxation is so slow that quasistatic properties are observed; this latter is known as the ''blocked'' state for the system. Midway between these two states, at the ''blocking temperature'' T_B, the times are equal, $\tau = \tau_m$. For a given ensemble T_B increases with decreasing measurement time. In typical experiments τ_m can range from the slow to medium time scales of 10^2 s for dc magnetization and 10^{-1}–10^{-5} s for conventional ac susceptibility, through to the fast time scales of 10^{-7}–10^{-9} s for ^{57}Fe Mössbauer spectroscopy. In each of these techniques the blocking temperature is associated with different features, such as peaks in the dc and ac susceptibility, and equivalent relative areas of sextet and doublet components in Mössbauer spectroscopy.

In the following we present the results of magnetic measurements over a variety of time scales on the granular alloy $Fe_{20}Cu_{20}Ag_{60}$.

B. Slow to medium time scales: dc magnetization, ac susceptibility, and *M-H* curves

1. dc magnetization

The thermal variation of the dc magnetization of the sample was recorded on a SQUID magnetometer using the standard zero-field-cooling–field-cooling (ZFC-FC) method. The sample temperature was changed at ~3 K min^{-1} and stabilized at each measuring point for approximately 2 min. Each data point was recorded as the average of three instrument scans, so that the measurement time was of order $\tau_m = 100$ s.

ZFC-FC curves were recorded for applied fields of $H = 50$ Oe, 500 Oe, and 1 kOe, and an additional FC curve was recorded for $H = 30$ kOe (see Fig. 4). In all cases the ZFC and FC curves coincide at 330 K, but diverge at lower temperatures. This splitting is often observed in fine particle and fine grain systems.[47] Had the sample been a bulk ferromagnet the ZFC and FC curves would have coincided and would have been largely flat, decreasing slightly with increasing temperature. The latter is expected from a Brillouin law reduction in magnetization with increasing temperature well below the Curie point, which for α-Fe is 1040 K. Although a

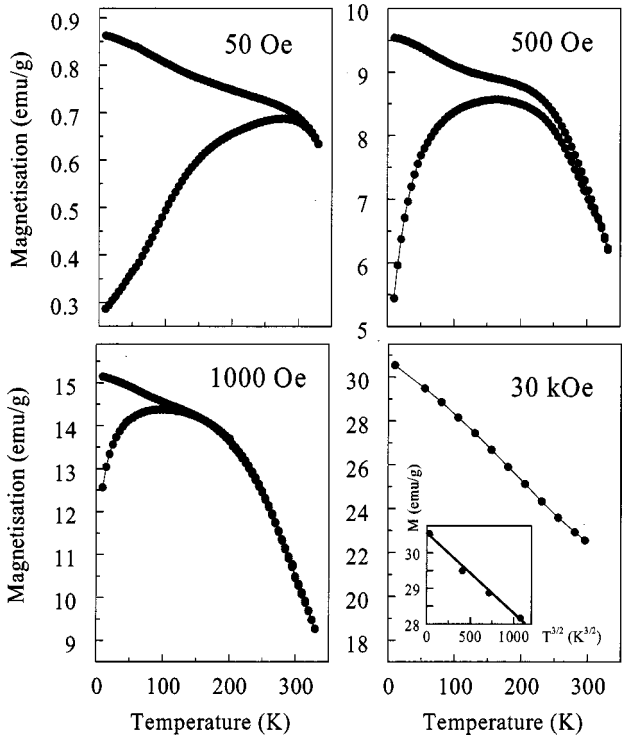

FIG. 4. dc magnetization data for an $Fe_{20}Cu_{20}Ag_{60}$ granular alloy. Zero-field-cooled (ZFC, lower) and field-cooled (FC, upper) curves are shown for applied fields of $H = 50$, 500, and 1000 Oe, and an FC curve only for $H = 30$ kOe. The splittings between the ZFC and FC curves, and the peaks in the ZFC curves, are typical of superparamagnetic systems. The reduction in FC magnetization with increasing temperature is larger than expected for bulk Fe-Cu grains, indicating that collective excitations are present—as exemplified by the initially linear dependence with $T^{3/2}$ shown in the inset for the $H = 30$-kOe data. This is also characteristic of nanoscale magnetic materials.

temperature-dependent reduction in magnetization is observed in the $Fe_{20}Cu_{20}Ag_{60}$ field-cooled data, it falls more strongly that can be attributed to the Brillouin curve alone. This divergence from Brillouin law behavior may be quantified by evaluating the parameter B in the thermal demagnetization Bloch $T^{3/2}$ law:

$$M(T) = M(0)[1 - BT^{3/2}]. \tag{2}$$

In the case of the $H = 30$-kOe FC curve, it is safe to assume that the sample is magnetically saturated, so that only thermal fluctuations contribute to $M(T)$, and the Bloch law is applicable. A reasonable Bloch law fit was obtained (Fig. 4), for $T \leqslant 150$ K, yielding $B \approx 6.5 \times 10^{-5}$ K$^{-3/2}$. This value is significantly larger than the B for bulk Fe, 3.4×10^{-6} K$^{-3/2}$,[54] in agreement with observations in other fine particle magnetic systems.[55] The enlarged B arises because the effects of surface phenomena are increased, and also because only long-wavelength spin waves can be excited.[56,57] Thus the spin waves can travel from one particle (or grain) to another rather than being confined within a given particle.

In the ZFC experiments the sample was cooled in zero field so that the directions of the net magnetizations of the grains became frozen at random. On subsequent heating in an applied field the grain magnetizations became ''unblocked'' (reoriented to lie parallel to the applied field) at temperatures that depended on the grain size and hence the anisotropy energy KV, and on the magnitude of the applied field. In the 50-Oe ZFC curve a broad peak in the magnetization has its maximum value at ~280 K, while in the 500- and 1000-Oe fields the somewhat less broad peaks have maxima at ~160 and 100 K, respectively. This variation with field is as expected, since a larger applied field induces moment reorientations at lower temperatures.

2. ac susceptibility

ac susceptibility (χ_{ac}) data were recorded from 5 to 350 K using an excitation field $h=10$ Oe and frequencies ν ranging from 50 to 3000 Hz. The main feature of both the in-phase (χ') and out-of-phase (χ'') data for these runs, shown in Fig. 5, was a broad peak with a 50-Hz maximum at $T_{max} \approx 285$ K for χ' and at $T_{max} \approx 230$ K for χ''. The position of the peak shifted slightly toward higher temperatures (290 and 240 K, respectively) when the measuring frequency was increased to 3000 Hz. The influence of superimposed longitudinal dc fields of 500 and 1000 Oe ($h=10$ Oe, $\nu=1000$ Hz), applied after cooling in zero field, is also shown in Fig. 5. The external field had a large effect on the susceptibility data, much more than a frequency change could produce, with the maxima shifting to lower temperatures ($\Delta T_{max}/T_{max} = -31\%$ for $H=500$ Oe, and -61% for $H=1000$ Oe, for the χ' curves) and the signal magnitude falling (e.g., by -36% in χ' between $H=0$ and $H=500$ Oe).

To better define the dynamical susceptibility behavior, further χ_{ac} runs for $\nu=30$ Hz, 1000 Hz, and 10 kHz were recorded at temperatures around the maxima (Fig. 5 inset). The change in T_{max} as a function of ν can be analyzed using several models dealing with the nature of the magnetic relaxation. Given the strong influence of an external field, we concentrate on the $H_{dc}=0$ data, which can then be compared directly with zero-field data from other techniques. For example, it is straightforward to extract the temperature shift per decade,[58] $T_{shift}=\Delta T_{max}/[T_{max}\cdot\Delta \log_{10}(\omega)]$, where $\omega=2\pi\upsilon$ is the angular measurement frequency. For $Fe_{20}Cu_{20}Ag_{60}$ $T_{shift} \approx 0.008$, which is smaller than the $T_{shift} \approx 0.10-0.12$ theoretically predicted for noninteracting fine particle systems.[58,59] The origin of this difference is most likely to be due to intergranular magnetic interactions.

To test this hypothesis, it is useful to consider other standard parameters extracted from the χ_{ac} data. (i) It is usual to characterize the activation process for the relaxation from the variation of T_{max} with measurement time $\tau_m=\upsilon^{-1}$. In dilute noninteracting systems, where the relaxation behavior is related to individual entities, the Arrhenius law, $\ln(\tau_m/\tau_0)=E_a/(k_B T_{max})$, is commonly found. However, in the case of $Fe_{20}Cu_{20}Ag_{60}$ a poor fit was obtained for the χ' data, with unphysical values for the parameters: $\tau_0 \approx 10^{-66}$ s and $E_a/k_B \approx 41\,600$ K. (ii) A less common procedure,[60] successfully tested in nonmetallic[24] and metallic[61] fine particle compounds, is to determine τ_0 from the $\chi''(T,\omega)$ data. According to the model, if the curves of $\chi''(T,\omega)$ plotted as a function of $-T\ln(\omega\tau_0)$ data can be made to collapse onto a single master curve, then the τ_0 of the relaxation can be defined. In the case of $Fe_{20}Cu_{20}Ag_{60}$, the lower frequency curves collapse for $\tau_0=10^{-17\pm1}$ s which is unrealistically small for a noninteracting system. (iii) Another approach, recently reported for melt-spun Co-Cu granular alloys,[61] and based on models of noninteracting fine particle systems,[62–64] is to relate the in-phase and out-of-phase susceptibilities according to

$$\chi'_{exp}(T) = -\frac{2}{\pi}\frac{\ln(\omega\tau_0)}{T}\int_0^T \chi''_{exp}(T)\,dT. \qquad (3)$$

The results for $Fe_{20}Cu_{20}Ag_{60}$ showed there was no clear reproduction of the χ' curves through the integration of the χ'' curves.

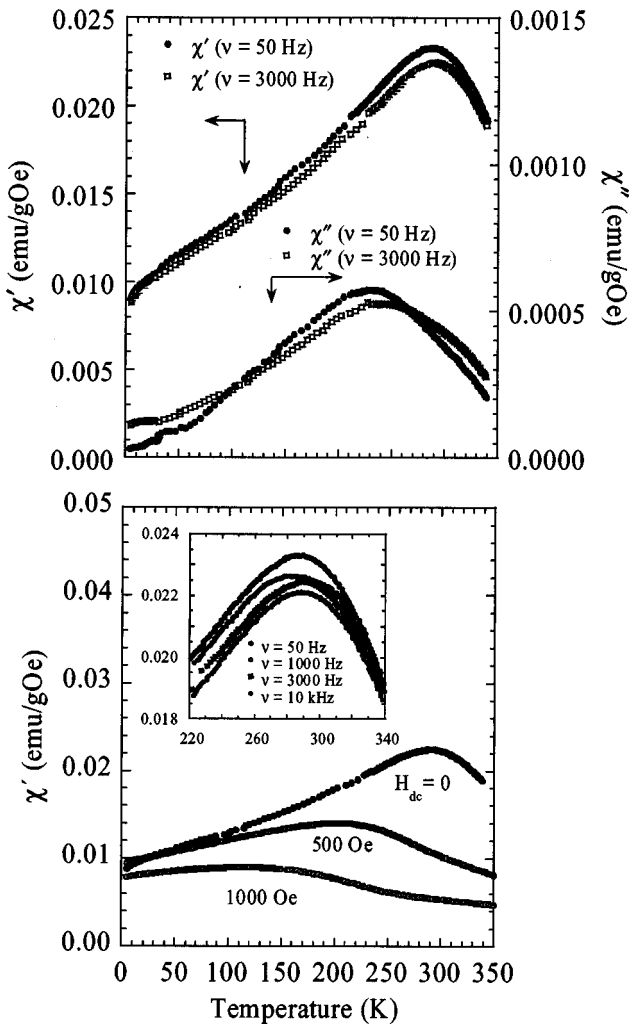

FIG. 5. In-phase (χ') and out-of-phase (χ'') ac susceptibility data for an $Fe_{20}Cu_{20}Ag_{60}$ granular alloy, with an excitation field of 10 Oe at frequencies of 50 and 3000 Hz (top). The relatively small peak shifts with frequency (shown at further frequencies in the inset) are typical of interacting fine grain systems. The large peak shifts and signal reduction seen in external dc fields of 500 and 1000 Oe (bottom) are also indicative of intergranular interactions.

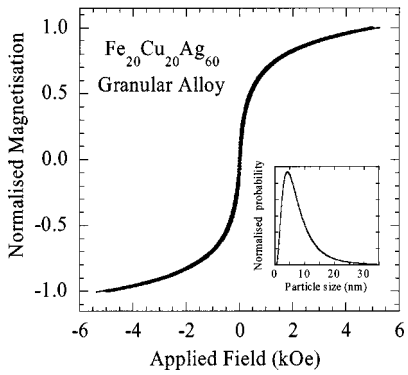

FIG. 6. Room-temperature *M-H* data for an $Fe_{20}Cu_{20}Ag_{60}$ granular alloy, showing the anhysteretic behavior typical of superparamagnetism. The solid curve superimposed on the data was calculated from a sum of Langevin functions for Fe-Cu grains of sizes following the log-normal distribution of the inset.

Together, these tests establish that the noninteracting models are not applicable to this alloy. Instead, we can test the nature of the magnetic relaxation mechanism by applying the phenomenological Vogel-Fulcher model, $\ln(\tau_m/\tau_0) = E_a/[k_B(T_{\max}-T_0)]$, to the measured peak temperatures as a function of measurement time. Such a model has previously been successfully applied to frequency-dependent susceptibility data from Co-Ag films.[65] In our case, when a physically realistic value of $\tau_0 = 10^{-11}$ s is selected as the attempt time for ferromagnetic particles, a reasonable fit is obtained, with realistic parameter values of $E_a/k_B \approx 320$ K and $T_0 \approx 270$ K. Thus overall, analysis of the ac susceptibility data shows that the high-temperature maxima are only feebly affected by frequency, while the activation processes involved can be related to the Vogel-Fulcher law. It was found to be impossible to describe the thermal variation of the susceptibility using models that assumed noninteracting systems.

3. M-H curves

Field-dependent magnetization data were recorded at room temperature in fields of up to 5 kOe (see Fig. 6). Anhysteretic traces were observed, indicating that the sample is superparamagnetic on the 1–10-s measurement time scale of the vibrating-sample magnetometer (VSM). This is in keeping with the dc magnetization and χ_{ac} experiments which also showed superparamagnetism at room temperature.

Anhysteretic *M-H* curves obtained above the superparamagnetic blocking temperature are typically modelled as a sum of Langevin functions:

$$M = M_s \sum_i w_i \left(\coth \beta_i - \frac{1}{\beta_i} \right), \quad \beta_i = \frac{\mu_i H}{kT}, \tag{4}$$

where M_s is the saturation magnetization, w_i is a probabilistic weighting factor, and μ_i is the volume-dependent moment of a given size distribution of magnetic grains.[66] From this it is possible to derive information on the distribution of grain sizes, usually by means of an assumed log-normal distribution:

$$F(y) = \frac{1}{\sigma y \sqrt{2\pi}} \exp\left[-\frac{\ln^2 y}{2\sigma^2} \right], \tag{5}$$

where $y = D/D_v$, D is the particle diameter, and D_v is the median diameter, and where σ is the standard deviation of the distribution.[66] Although Eq. (4) is based on an assumption of little or no interaction between the magnetic grains, recent work has shown that it can be successfully applied to even strongly interacting systems, in the superparamagnetic region.[67] In any case, the dc magnetization data on our $Fe_{20}Cu_{20}Ag_{60}$ sample indicates that a field of 500 Oe can shift the ZFC peak temperature from 280 to 160 K, so it is reasonable to expect that in moderately large fields (e.g., $\geqslant$1 kOe) the *M-H* curve response will be dominated by the temperature-dependent fluctuations of the nanoscale grains.

Fitting the room-temperature data yielded the fit shown as a solid curve in Fig. 6. For the fit a 35-box histogram of grain sizes from 1 to 35 nm was used, with the density of the grains taken as 7.91 g cm^{-3} from the x-ray data. The moments of the grains were computed using a fitted value for the uniform Fe-Cu saturation magnetization of 620 emu cm^{-3}. This latter value compares favorably with a value of $\sim$600 emu cm^{-3} for a room-temperature *M-H* curve of ball milled $Fe_{50}Cu_{50}$. The fitted distribution parameters were $D_v = 6.6 \pm 0.1$ nm and $\sigma = 0.67 \pm 0.01$, giving the log-normal curve shown as an inset in Fig. 6. The most probable grain size is 4.2 nm, which is in good agreement with the 5.5 $\pm$0.5-nm value found in the Rietveld analysis.

C. Fast time scales: Mössbauer spectroscopy

^{57}Fe Mössbauer spectra were recorded in zero field at 80 K and room temperature, and in an applied field of 11 kOe at room temperature (see Fig. 7). The relatively poor statistical quality of the spectra can largely be attributed to the relatively small Fe content in the sample, allied to the relatively high electronic mass absorption coefficient of Ag (44 cm^2 g^{-1} compared to 64 cm^2 g^{-1} for Fe). This problem is exacerbated by the relatively large mean size of the alloyed particles (most having diameters of order 30–50 μm as measured by SEM), which exceeds the 20-μm ideal thickness for γ-ray transmission through $Fe_{20}Cu_{20}Ag_{60}$. Nevertheless, some very clear and significant features are apparent in the spectra.

The zero-field room-temperature spectrum comprises a doublet and a broad singlet. It is impossible to tell from this spectrum alone whether the sample is in a superparamagnetic or a paramagnetic state. However, the spectrum obtained in an applied field of 11 kOe shows unambiguously that the sample is superparamagnetic. A magnetically split sextet is obtained, with a mean *effective* field (arising from the vector addition of the hyperfine field and applied field) of order 196 kOe, which is much larger than the 11-kOe field that would have been observed had the sample been paramagnetic. Thus the zero-field spectrum must correspond to nanoscale supermoments relaxing at time scales faster than or close to the Mössbauer measurement time, which in α-Fe is of order 2×10^{-8}s. The zero-field 80-K spectrum also comprises a magnetically split sextet, implying that at this reduced tem-

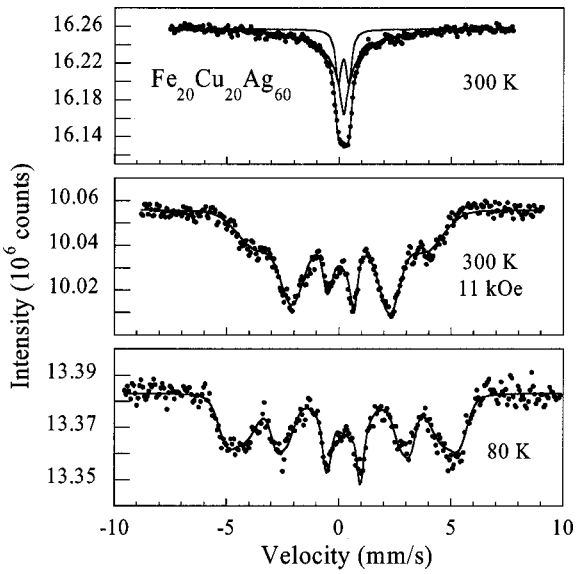

FIG. 7. ^{57}Fe Mössbauer spectra for an $Fe_{20}Cu_{20}Ag_{60}$ granular alloy recorded at room temperature in zero field and in an 11-kOe external field applied perpendicular to the γ-ray beam direction, and at 80 K in zero field. The solid lines show the results of least-squares fits of the data to a dynamic relaxation model (300 K, zero field) and to a static hyperfine field distribution model (300 K, 11 kOe, and 80 K, zero field). The data unambiguously prove that the sample is superparamagnetic, with an average superparamagnetic relaxation time of less than 10^{-8} s at room temperature.

perature the supermoment fluctuations have slowed down so that they are static on the Mössbauer time scale. The mean hyperfine field at 80 K is of order 255 kOe, which is consistent with the anticipated increase in hyperfine field with decreasing temperature, starting from a value of order 207 kOe (obtained from the mean effective field, recalling that the hyperfine field in Fe aligns antiparallel to the applied field) at room temperature.

Given this interpretation, the 80 K and room-temperature applied field spectra were fitted using a Voigtian based static distribution model[68] to get the parameters listed in Table II and the solid line fits shown in Fig. 7. The $P(H)$ hyperfine field distributions are broad and asymmetric, as expected for nanoscale $Fe_{60}Cu_{40}$ grains in which a relatively large proportion of Fe atoms reside at or near the interface with the Ag matrix, thereby experiencing a smaller hyperfine field than those Fe atoms in the center of the grains. A phenomenological approach was used to construct the asymmetric $P(H)$ distributions from symmetric Gaussian $P(H)$ distributions—three such Gaussians were used for the 80-K spectrum, two for the 300-K applied field spectrum. The parameters of these component Gaussian distributions are listed in Table II. The weighted mean hyperfine fields are smaller than for pure α-Fe, due to the disrupting effect of the alloyed Cu atoms on the Fe-Fe exchange interactions. The room-temperature mean field of 207 kOe is close to the 222-kOe mean field measured previously in ball milled $Fe_{50}Cu_{50}$.[29]

Returning to the zero-field room-temperature spectrum, we can, for illustrative purposes, fit it using a dynamic Lorentzian line-shape model[69,70] in which a single-valued hyperfine field is assumed to jump randomly between two directions on the same axis at an average jump frequency f. Although the real situation in the sample is undoubtedly more complex, it is nevertheless informative in that we can see that both the singlet and doublet components may be generated by a superparamagnetically fluctuating hyperfine field—which, following our previous analysis, we take to be of magnitude 207 kOe. The doublet component, assumed to correspond to those grains in the sample that were in a fully superparamagnetic state, were assigned a large jump frequency $f=10^{14}$ Hz so that the time-averaged hyperfine field

TABLE II. ^{57}Fe Mössbauer parameters for an $Fe_{20}Cu_{20}Ag_{60}$ granular alloy as determined by (i) Voigtian based line profile analysis of static hyperfine parameter distributions in the 80-K and applied field 300-K spectra, and (ii) dynamic Lorentzian line-shape analysis for the magnetically relaxing zero-field 300-K spectrum. The parameters listed are: isomer shift δ (mms^{-1}), quadrupole shift 2ε (mms^{-1}), hyperfine field H and mean hyperfine field $\langle H\rangle$ (kOe), Gaussian standard deviation on the Voigt profile hyperfine field distributions σ_H (kOe), relaxation frequency f (Hz), and subcomponent populations p (%). For the 300-K applied field spectrum, $\langle H\rangle$ refers to the effective field obtained from the vector addition of the hyperfine and applied fields. Parameters marked with an asterisk were constrained to the given value during the fit.

Voigtian analysis (static distribution)

Spectrum	δ	$\langle H\rangle$	σ_H	p
80 K, zero field	0.36 (12)	274 (33)	31 (19)	53 (1)
		323 (16)	19 (12)	31 (5)
		60 (13)	39 (20)	16 (3)
300 K, 11 kOe	0.21 (7)	235 (7)	48 (10)	68 (5)
		100 (25)	90 (30)	32 (5)

Dynamic Lorentzian analysis (magnetically relaxing)

Spectrum	δ	2ε	f	H	p
300 K, zero field	0.20 (2)	0*	$3.0(4)\times10^8$	207*	75 (5)
	0.19 (1)	0.46 (2)	10^{14}*	207*	25 (3)

for this component was zero. The broad singlet component was fitted to a jump frequency of $f \approx 3.0 \times 10^8$ Hz, which is of the same order as the inverse measurement time, $\tau_m^{-1} \approx 8 \times 10^7$ Hz, for a hyperfine field of 207 kOe, thus explaining the broad nature of the resolved spectrum.

We can tentatively estimate the Mössbauer blocking temperature from the data at hand. The zero-field room-temperature spectrum comprises 25% superparamagnetic doublet plus a 75% slowly relaxing component. Given that the Mössbauer T_B is defined as the temperature at which the superparamagnetic fraction accounts for half of the spectral area, we can conclude that T_B must be greater than 300 K. However, it should be noted that the measured superparamagnetic fraction can be model dependent. Also, a more complete set of temperature-dependent Mössbauer spectra would allow a more reliable value of T_B to be obtained. With the present data it is perhaps safest to conclude simply that the average superparamagnetic relaxation time in the sample is less than $\sim 10^{-8}$ s at room temperature.

D. Intermediate time scales: μSR spectroscopy

In muon spin relaxation experiments, spin polarized muons are implanted into the sample, where they precess about any local field not parallel with their initial polarization.[71,72] Any variation in site or field strengths within the sample leads to the dephasing of the precession motions, and the net depolarization of the spins.

With an average lifetime of 2.2 μs, after implantation the muon decays into a positron and two neutrinos. The positron is emitted preferentially in the direction of the muon polarization, and at ISIS is picked up by forward and backward detectors in $\pm z$, where z is the direction on travel of the incident muon beam. The positron emission distribution is $1 + a \cos\theta$, where $a \approx 0.3$ is a constant. The zero field μSR function $G_z(t)$ is extracted from the positron histograms in the forward and backward detectors, $N_F(t)$ and $N_B(t)$, by taking the ratio

$$P(t) = a_0 G_Z(t) = \frac{N_F(t) - \alpha N_B(t)}{N_F(t) + \alpha N_B(t)}, \tag{6}$$

where α is an instrumental parameter to account for different detector efficiencies, and a_0 is the initial asymmetry, typically 0.21–0.25.

$P(t)$ curves were measured for the $Fe_{20}Cu_{20}Ag_{60}$ sample as a function of temperature from 10 to 350 K in zero field (see Fig. 8), and at selected temperatures in longitudinal applied fields (parallel to the z axis) of 500 and 2000 Oe (see Fig. 9). Several different functional forms were tested in fitting the depolarization curves. The best fit was obtained using a simple phenomenological model of two exponentially decaying signals (a_1 and a_2) plus a constant offset signal (a_f):

$$P(t) = a_1 \exp(-\lambda_1 t) + a_2 \exp(-\lambda_2 t) + a_f, \tag{7}$$

where the a_f parameter included contributions both from the sample and from the silver plate on which the sample was mounted. Solid lines corresponding to these fits are shown in Figs. 8 and 9, and selected data on the fitted parameters are shown in Fig. 10 and in Table III. [Note that there is a difference of ~2.5% between the a_f asymmetry found in the data in (i) Figs. 8 and 10, and (ii) Fig. 9 and Table III. This arises because the data were recorded on different spectrometers and had different baseline signals—largely due to the silver mounting plates used.] The zero-field data show a peak in both of the exponential relaxation rates, λ_1 and λ_2, at 275 K, and a sharp rise in the initial asymmetry a_0 (where $a_0 = a_1 + a_2 + a_f$) at $T \geqslant 275$ K. We note that these features are visible in the raw data. This can be seen in Fig. 8 where the depolarization curve at 275 K is almost flat beyond 3–4 μs, while at both 250 and 300 K a downward slope persists at these longer times—a manifestation of the peak in λ_1 and λ_2. Also, the slope of the curves in the first 0.5 μs becomes much steeper at and above 275 K, which corresponds to the increase in a_0.

The transition in the muon data at around 275 K is confirmed by the applied field measurements (Fig. 9 and Table III). In particular, the applied field affects the final asymme-

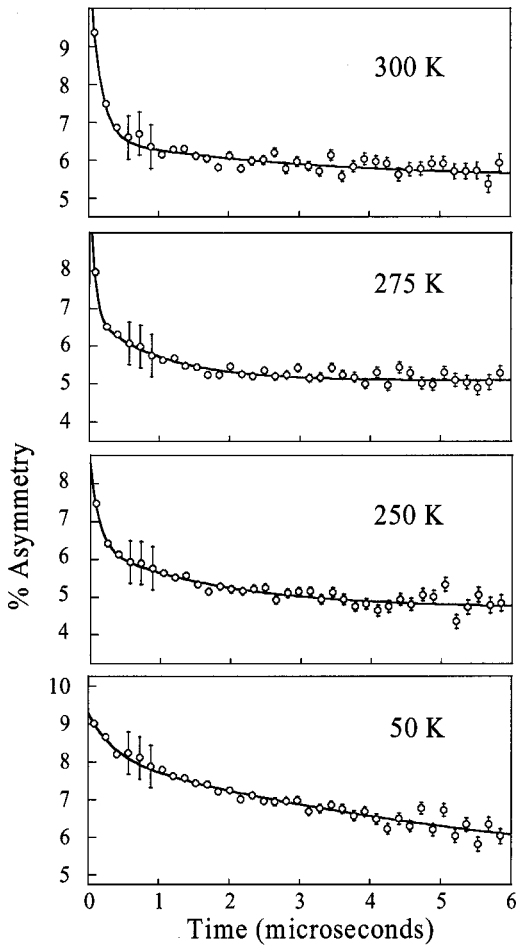

FIG. 8. Zero-field muon spin relaxation spectra of an $Fe_{20}Cu_{20}Ag_{60}$ granular alloy as a function of temperature. The solid lines are the results of fits to a phenomenological model comprising two exponential decays and a constant offset. A change in behavior at 275 K, where the curve flattens out beyond $t \approx 3-4$ μs, is evidence of a superparamagnetic blocking transition. The increased noise level near $t = 0.8$ s is an instrumental effect.

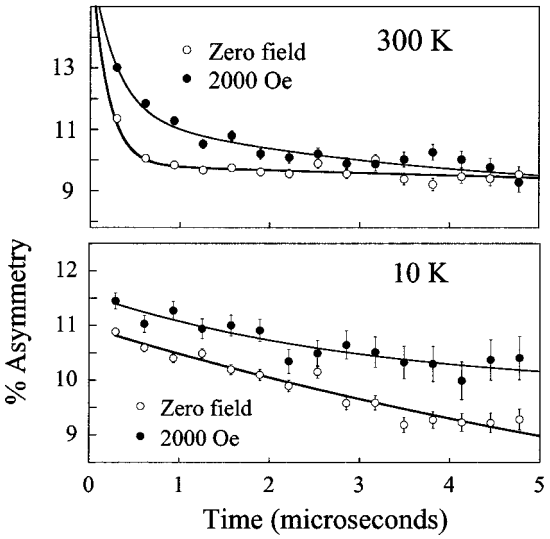

FIG. 9. Muon spin relaxation spectra of an $Fe_{20}Cu_{20}Ag_{60}$ granular alloy at 10 and 300 K in zero field and in a longitudinal applied field of 2000 Oe. The solid lines are fits to a model comprising two exponential decays and a constant offset. The divergence of the curves as a function of time at 10 K is evidence of static behavior (below the blocking temperature T_B), and the convergence of the curves at 300 K is evidence of dynamic behavior (above T_B).

try parameter a_f, which increases at 10 and 100 K, is unchanged at 250 K, and decreases at 300 K. The increase in a_f at 10 K is a signature of a static magnetic environment, in which the local fields about which the muons precess are brought closer to the initial polarization direction through the vectorial addition of the applied field. The decrease in a_f at 300 K is a sign of a rapidly fluctuating (superparamagnetic) environment. In zero field at 300 K, some or all of the implanted muons are unable to establish a coherent precession with the rapidly fluctuating local field—a feature evidenced

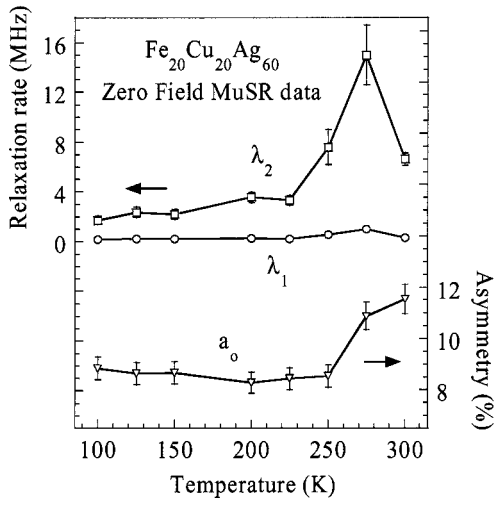

FIG. 10. Temperature dependence of selected parameters from fits of the zero-field μSR data of Fig. 8. The peaks in the relaxation rates λ_1 and λ_2, and the sharp increase in the initial asymmetry a_0, indicate a superparamagnetic blocking temperature of approximately 275 K.

by the increase in a_f at 275 K and above (Fig. 10). The effect of the applied field is to slow down the flipping rates for the local fields so that more muons are able to depolarize, resulting in a reduction in the final asymmetry.

The muon data are therefore consistent with the other techniques in the observation of a blocking transition. The blocking temperature may be tentatively placed at 275 ± 15 K, confirming that the blocking temperature changes only slightly as a function of measurement time in this alloy, as has also been shown by the ac susceptibility results.

V. DISCUSSION

The selected $Fe_{20}Cu_{20}Ag_{60}$ alloy is shown by EDAX and elemental analysis to be homogeneous at the instrumental resolution scale of a micron. Rietveld refinement of synchrotron x-ray-diffraction data shows that on average it comprises 5-nm bcc $Fe_{60}Cu_{40}$ alloy grains in a matrix of 4-nm fcc $Ag_{90}Cu_{10}$ grains, with both the magnetic grains and the matrix subject to relatively large strains, of order 8 and 6 %, respectively. The observation of only a small (1–2 wt %) pseudoamorphous grain-boundary contribution is consistent with the boundaries being relatively thin, less than ~1 nm thick.[41,46] An estimate of the distribution of magnetic grain sizes is obtained by analyzing the anhysteretic room-temperature *M-H* curve, giving a median size ~7 nm and a most probable size ~4 nm.

Given such fine scale grains, it might have been expected that superparamagnetic blocking transitions would be found at relatively low temperatures. Indeed, for noninteracting superparamagnetic α-Fe particles with mean sizes of up to 8 nm, blocking temperatures below 50 K are predicted[73] for even the fastest of the measurement techniques (viz., Mössbauer spectroscopy) used in this study. However, the measured blocking temperatures are much higher than this, e.g., above room temperature as measured by Mössbauer spectroscopy. There is also a notably small frequency dependence of the observed blocking behavior, e.g., the peak temperatures measured by ac susceptibility vary only from ~285 K at a measurement frequency of 50 Hz, to ~290 K at 3000 Hz. This is much smaller than is usually seen in noninteracting systems.[58,59]

The elevated blocking temperatures are a sign that the average energy barrier to moment reversal, $\Delta E = KV$, is larger than expected. One possible explanation for this is that the anisotropy energy constant K is enhanced compared to that usually found in α-Fe nanoparticles. Such an effect is entirely plausible, both because the anisotropy of an Fe-Cu alloy grain will not be the same as that of a pure Fe grain, and because it is well known that K may be affected by grain size, shape, stress, strain, and surface effects.[10,47] However, an enhanced anisotropy constant cannot account for the relatively feeble frequency dependence of the observed blocking transitions, as characterized by the parameter $T_{\text{shift}} \approx 0.008$ from the ac susceptibility data. The most likely causes for such behavior are intergranular interactions.[47] In particular, similarly small values of T_{shift} have been identified by Mørup and co-workers[74] as a sign of a spin-glass-like ordering transition, i.e., one involving the co-operative freezing of the

TABLE III. Muon spin relaxation parameters for an $Fe_{20}Cu_{20}Ag_{60}$ granular alloy as determined by fitting a series of spectra recorded as a function of temperature and longitudinal applied field (some of which are shown in Fig. 9). A phenomenological model was used in which the depolarization was fitted as $P(t) = a_1 \exp(-\lambda_1 t) + a_2 \exp(-\lambda_2 t) + a_f$. An initial asymmetry parameter is listed; it is defined as $a_0 = a_1 + a_2 + a_f$.

Temperature (K)	Applied field (Oe)	Initial asymmetry a_0 (%)	Final asymmetry a_f (%)	Relaxation rate λ_1 (MHz)	Fast relaxation asymmetry a_2 (%)	Relaxation rate λ_2 (MHz)
10	0	11.0(1)	6.0(8)	0.10(2)		
	2000	11.6(2)	9.8(4)	0.32(16)		
100	0	12.9(9)	6.5(2)	0.29(4)	2.3(8)	5.2(19)
	500	12.0(3)	7.4(2)	0.27(5)	1.2(3)	2.7(13)
250	0	10.6(1)	6.8(2)	0.32(13)	2.5(3)	3.2(8)
	500	11.3(3)	6.7(3)	0.25(14)	3.3(3)	2.8(5)
300	0	18(3)	8.5(1)	0.82(27)	8.0(27)	8.4(22)
	500	14(1)	7.2(1)	0.65(16)	5.1(8)	5.6(12)
	2000	12.5(9)	4.8(4)	0.28(13)	5.0(8)	3.6(10)

magnetic moments. Such behavior is intuitively reasonable given the relatively large amount of magnetic material in the alloy. In fact, other authors have proposed the existence of a spin-glass magnetic phase in Co-Cu granular alloys.[25] Recent dc magnetization and ac susceptibility measurements[75] in mechanically alloyed $Fe_{20}Cu_{21}Al_{49}$ show similar findings to ours, and are said to manifest the importance of interactions between particles in the blocking process, with spin-glass-like features. Similarly, current work[76] on the role of intergranular (or interparticle) interactions in nanoscale systems has shown, for simple samples based on Fe-C amorphous ferrofluids, that increased sample concentration (with increased interparticle interactions) gives rise to transitions of a spin-glass-like nature.

The most common sources of interactions between magnetic grains or particles diluted in a solid matrix are: exchange, dipole-dipole, and Ruderman-Kittel-Kasuya-Yosida (RKKY).[10] Exchange coupling across grain boundaries containing magnetic atoms is thought to be a significant factor in determining the magnetism of the nanocrystalline Fe-Zr-Cu-B and Fe-Nb-Cu-Si-B alloys, where Fe grains are embedded in a ferromagnetic or paramagnetic matrix.[7,77] The situation is different in the $Fe_{20}Cu_{20}Ag_{60}$ alloy, where the diamagnetic nature of the Ag matrix does not lend itself to any exchange mechanism between Fe-Cu grains. However, the thin (less than $\sim$1 nm) grain boundaries mean that if the spatial distribution of the Fe-Cu grains in the Ag matrix is not homogeneous, neighboring magnetic grains might be close enough to one another to exchange couple. As well as exchange, throughout the sample the weaker but more long-range dipole-dipole interactions will be present, while the metallic matrix is capable of supporting RKKY (indirect oscillatory exchange) coupling between grains. Calculations of the interaction energy between ferromagnetic entities in a nonmagnetic matrix show that the oscillatory character of the indirect exchange is retained.[78] Recent theoretical considerations of Co clusters in a Cu matrix show that the RKKY interactions are dominant for all intercluster distances when those clusters are very small (1 nm), whereas the dipolar interaction becomes increasingly important for larger sizes.[79] We conclude from this that although it is certain that all three interactions are present and combine in a complicated manner in the alloy, the dipolar interactions are more likely to be dominant in regions where the magnetic grains are well separated, while the exchange interactions will be dominant in regions where the magnetic grains are clustered.

VI. CONCLUSIONS

Conventional studies of superparamagnetism and other fast relaxation effects have almost exclusively been focused on near-ideal samples of monodisperse fine particles or grains supported on or dispersed in a nonmagnetic medium. However, materials including those exhibiting GMR and those with ultrasoft magnetic properties such as the ''nanocrystalline'' alloys, also exhibit fast magnetic relaxation effects. In this paper we have characterized the magnetic relaxation properties of a member of a family of fine grained alloys, the Fe-Cu-Ag alloys, as a representative of this class of technologically relevant nanophase materials.

(i) The alloy chosen had the composition $Fe_{20}Cu_{20}Ag_{60}$ and comprised a dispersion of bcc $Fe_{60}Cu_{40}$ grains of mean size $\sim$5.5 nm in an fcc $Ag_{90}Cu_{10}$ matrix. It had a GMR-like field-dependent resistivity, with a magnetoresistive ratio at room temperature of $\sim$5% in a 90-kOe field. DSC measurements showed that on heating to temperatures above 380 K the sample began a structural rearrangement, with the onset of decomposition and recrystallization. This set an operational working limit of $\sim$350 K on the magnetic relaxation experiments.

(ii) dc magnetization and ac susceptibility measurements both showed a peak typical of superparamagnetic materials, but with much higher blocking temperatures than would be expected from 5.5-nm-sized Fe-Cu grains. The dynamical behavior of the susceptibility peak corresponded to a Vogel-Fulcher process and the thermal variation of the curves could not be interpreted according to a noninteracting model.

(iii) Mössbauer experiments in zero field at 300 K showed

a superparamagnetic doublet and a slowly relaxing broad singlet. The application of an 11-kOe field was found to be sufficient to keep the supermoments static on the Mössbauer time scale, revealing a magnetically split sextet. This unambiguously proved the superparamagnetic nature of the sample.

(iv) Experiments using the relatively uncommon technique of μSR spectroscopy gave results in keeping with the other methods. In particular, a peak was seen in the exponential decay rates of the muon depolarization spectra, which confirmed the existence of a blocking transition on the muon time scale. This result establishes the feasibility of the μSR technique as a way of analyzing nanoscale magnetic systems, with the added advantage that measurements can be conducted in absolutely zero field.

Taken together the data constitute a consistent set of measurements of the relaxation behavior of a strongly interacting ensemble of nanoscale magnetic grains in a technologically important granular alloy.

ACKNOWLEDGMENTS

We thank the British Council and the Spanish CICYT for their support of this work under an Acciones Integradas collaborative grant; W. A. Steer (University College London) and M. Roberts (Daresbury Laboratory) for collecting the x-ray data; N. S. Cohen (University of London Intercollegiate Research Service) for performing the DSC run; and J. M. Barandiarán (Universidad del País Vasco), F. J. Lázaro (Universidad de Zaragoza), E. M. Forgan (University of Birmingham), and S. Enzo (Università degli Studi de Sassari) for helpful discussions and advice.

*Corresponding author. Email address: q.pankhurst@ucl.ac.uk

[1] G. C. Hadjipanayis and R. W. Siegel, *Nanophase Materials: Synthesis, Properties, Applications* (Kluwer Academic, Dordrecht, 1994).

[2] J. L. Dormann and D. Fiorani, *Magnetic Properties of Fine Particles* (North-Holland, Amsterdam, 1992).

[3] G. Herzer, in *Handbook of Magnetic Materials*, edited by K. H. J. Buschow (Elsevier, Amsterdam, 1997), Vol. 10, p. 415.

[4] K. Suzuki, A. Makino, A. Inoue, and T. Masumoto, J. Appl. Phys. **70**, 6232 (1991).

[5] A. Slawska-Waniewska and J. M. Greneche, Phys. Rev. B **56**, R8491 (1997).

[6] J. Arcas, A. Hernando, J. M. Barandiaran, C. Prados, M. Vazquez, P. Marin, and A. Neuweiler, Phys. Rev. B **58**, 5193 (1998).

[7] T. Kemeny, J. Balogh, I. Farkas, D. Kaptas, L. F. Kiss, T. Pusztai, L. Toth, and I. Vincze, J. Phys.: Condens. Matter **10**, L221 (1998).

[8] J. S. Garitaonandia, D. S. Schmool, and J. M. Barandiaran, Phys. Rev. B **58**, 12 147 (1998).

[9] D. Kaptas, T. Kemeny, J. Balogh, L. Bujdoso, L. F. Kiss, T. Pusztai, and I. Vincze, J. Phys.: Condens. Matter **11**, L179 (1999).

[10] A. Hernando, J. Phys.: Condens. Matter **11**, 9455 (1999).

[11] J. S. Garitaonandia, P. Gorria, L. Fernández Barquín, and J. M. Barandiaran, Phys. Rev. B **61**, 6150 (2000).

[12] J. Q. Wang and G. Xiao, Phys. Rev. B **49**, 3982 (1994).

[13] C. B. Peng and D. S. Dai, J. Appl. Phys. **76**, 2986 (1994).

[14] J. P. Wang, H. L. Luo, N. F. Gao, and Y. Y. Liu, J. Mater. Sci. **31**, 727 (1996).

[15] M. M. P. de Azevedo, J. B. Sousa, J. A. Mendes, B. G. Almeida, M. S. Rogalski, Y. G. Pogorelov, I. Bibicu, L. M. Redondo, M. F. da Silva, C. M. Jesus, J. G. Marques, and J. C. Soares, J. Magn. Magn. Mater. **173**, 230 (1997).

[16] A. Hernando, C. Gomez Polo, M. El Ghannami, and A. G. Escorial, J. Magn. Magn. Mater. **173**, 275 (1997).

[17] P. Nash, R. B. Schwarz, and M. F. Hundley, Nanostruct. Mater. **10**, 893 (1998).

[18] O. Redon, J. Pierre, B. Rodmacq, B. Mevel, and B. Dieny, J. Magn. Magn. Mater. **149**, 398 (1995).

[19] N. S. Cohen, Q. A. Pankhurst, and L. Fernández Barquín, Hyperfine Interact. **3**, 285 (1998).

[20] A. Maeda, M. Kume, S. Oikawa, and K. Kuroki, Jpn. J. Appl. Phys., Part 1 **33**, 4919 (1994).

[21] F. Bødker, S. Mørup, C. A. Oxborrow, S. Linderoth, M. B. Madsen, and J. W. Niemantsverdriet, J. Phys.: Condens. Matter **4**, 6555 (1992).

[22] F. Bødker, S. Mørup, M. S. Pedersen, P. Svedlindh, G. T. Jonsson, J. L. GarciaPalacios, and F. J. Lázaro, J. Magn. Magn. Mater. **177**, 925 (1998).

[23] Y. Park, S. Adenwalla, G. P. Felcher, and S. D. Bader, Phys. Rev. B **52**, 12 779 (1995).

[24] F. J. Lázaro, J. L. Garcia, V. Schunemann, C. Butzlaff, A. Larrea, and M. A. Zaluska-Kotur, Phys. Rev. B **53**, 13 934 (1996).

[25] J. R. Childress and C. L. Chien, Phys. Rev. B **43**, 8089 (1991).

[26] B. J. Hickey, M. A. Howson, S. O. Musa, G. J. Tomka, B. D. Rainford, and N. Wiser, J. Magn. Magn. Mater. **147**, 253 (1995).

[27] F. J. Lázaro, A. Lopez, A. Larrea, Q. A. Pankhurst, J. M. L. Nieto, and A. Corma, IEEE Trans. Magn. **34**, 1030 (1998).

[28] B. Idzikowski, U. K. Rossler, D. Eckert, K. Nenkov, and K. H. Muller, Europhys. Lett. **45**, 714 (1999).

[29] N. S. Cohen, E. Ahlswede, J. D. Wicks, and Q. A. Pankhurst, J. Phys.: Condens. Matter **9**, 3259 (1997).

[30] Q. A. Pankhurst, N. S. Cohen, and M. Odlyha, J. Phys.: Condens. Matter **10**, 1665 (1998).

[31] D. H. Ucko, N. S. Cohen, L. Fernández Barquín, and Q. A. Pankhurst (unpublished).

[32] L. Cristofolini, K. Prassides, K. Vavekis, A. Amato, F. N. Gygax, A. Schenck, S. Gider, and D. D. Awschalom, Hyperfine Interact. **104**, 269 (1997).

[33] R. I. Bewley and R. Cywinski, J. Magn. Magn. Mater. **177**, 923 (1998).

[34] R. I. Bewley and R. Cywinski, Phys. Rev. B **58**, 11 544 (1998).

[35] T. Prokscha, M. Birke, E. Forgan, H. Glucker, A. Hofer, T. Jackson, K. Kupfer, J. Litterst, E. Morenzoni, C. Niedermayer, M. Pleines, T. Riseman, A. Schatz, G. Schatz, H. P. Weber, and C. Binns, Hyperfine Interact. **121**, 569 (1999).

[36] E. M. Forgan, T. J. Jackson, T. M. Riseman, H. Gluckler, E. Morenzoni, T. Prokscha, H. P. Weber, A. Hofer, C. Niedermayer, G. Schatz, M. Birke, H. Luetkens, J. Litterst, A. Schatz, and C. Binns, Physica B **289**, 137 (2000).

[37] T. J. Jackson, C. Binns, E. M. Forgan, E. Morenzoni, C. Niedermayer, H. Gluckler, A. Hofer, H. Luetkens, T. Prokscha, T. M.

Riseman, A. Schatz, M. Birke, J. Litterst, G. Schatz, and H. P. Weber, J. Phys.: Condens. Matter **12**, 1399 (2000).
[38] J. Rodríguez Carvajal, Satellite Meeting XVth Congress Int. Union of Crystallography (unpublished), p. 127.
[39] J. Rodríguez Carvajal, Physica B **192**, 55 (1993).
[40] F. L. Pratt, Physica B **289**, 710 (2000).
[41] H. Guerault and J. M. Greneche, J. Phys.: Condens. Matter **12**, 4791 (2000).
[42] W. H. Hall and G. K. Williamson, Proc. Phys. Soc. London, Sect. B **64**, 937 (1951).
[43] S. Enzo, R. Frattini, R. Gupta, P. P. Macri, G. Principi, L. Schiffini, and G. Scipione, Acta Mater. **44**, 3105 (1996).
[44] C. Suryanarayana and M. Grant Norton, *X-Ray Diffraction: A Practical Approach* (Plenum, New York, 1998).
[45] D. L. Leslie-Pelecky and R. L. Schalek, Phys. Rev. B **59**, 457 (1999).
[46] C. N. Chinnasamy, A. Narayanasamy, N. Ponpandian, K. Chattopadhyay, H. Guerault, and J. M. Greneche, J. Phys.: Condens. Matter **12**, 7795 (2000).
[47] J. L. Dormann, D. Fiorani, and E. Tronc, Adv. Chem. Phys. **98**, 283 (1997).
[48] L. Néel, Ann. Geophys. (C.N.R.S.) **5**, 99 (1949).
[49] W. F. Brown, Jr., Phys. Rev. **130**, 1677 (1963).
[50] E. Tronc, P. Prene, J. P. Jolivet, F. Dorazio, F. Lucari, D. Fiorani, M. Godinho, R. Cherkaoui, M. Nogues, and J. L. Dormann, Hyperfine Interact. **95**, 129 (1995).
[51] C. Johansson, M. Hanson, M. S. Pedersen, and S. Mørup, J. Magn. Magn. Mater. **173**, 5 (1997).
[52] M. Garcia del Muro, X. Batlle, A. Labarta, J. M. Gonzalez, and M. I. Montero, J. Appl. Phys. **81**, 3812 (1997).
[53] E. F. Ferrari, F. C. S. daSilva, and M. Knobel, Phys. Rev. B **56**, 6086 (1997).
[54] B. E. Argyle, S. H. Charap, and E. P. Pugh, Phys. Rev. **132**, 2051 (1963).
[55] C. B. Peng, S. Zhang, G. Z. Li, and D. S. Dai, J. Appl. Phys. **76**, 998 (1994).
[56] C. Kittel, *Quantum Theory of Solids* (Wiley, New York, 1963).
[57] X. Batlle, M. G. del Muro, and A. Labarta, Phys. Rev. B **55**, 6440 (1997).
[58] J. A. Mydosh, *Spin Glasses* (Taylor & Francis, London, 1993).
[59] J. L. Dormann, L. Bessais, and D. Fiorani, J. Phys. C **21**, 2015 (1988).
[60] A. Labarta, O. Iglesias, L. Balcells, and F. Badia, Phys. Rev. B **48**, 10 240 (1993).
[61] A. Lopez Polo, F. J. Lázaro, R. von Helmolt, J. L. Garcia Palacios, J. Wecker, and H. Cerva, J. Magn. Magn. Mater. **187**, 221 (1998).
[62] M. I. Shliomis and V. I. Stepanov, in *Relaxation Phenomena in Condensed Matter*, edited by W. Coffey (Wiley, New York, 1994), p. 1.
[63] J. L. Garcia Palacios, Ph.D. thesis, Universidad de Zaragoza, 1998.
[64] A. Lopez Polo, Ph.D. thesis, Universidad de Zaragoza, 1999.
[65] S. B. Slade, F. T. Parker, and A. E. Berkowitz, J. Appl. Phys. **75**, 6613 (1994).
[66] R. W. Chantrell, J. Popplewell, and S. W. Charles, IEEE Trans. Magn. **MAG-14**, 975 (1978).
[67] G. F. Goya, H. R. Rechenberg, and J. Z. Jiang, J. Magn. Magn. Mater. **218**, 221 (2000).
[68] D. G. Rancourt and J. Y. Ping, Nucl. Instrum. Methods Phys. Res. B **58**, 85 (1991).
[69] M. Blume and J. A. Tjon, Phys. Rev. **165**, 446 (1968).
[70] D. G. Rancourt, in *Mössbauer Spectroscopy Applied to Magnetism and Materials Science*, edited by G. J. Long and F. Grandjean (Plenum, New York, 1996), Vol. 2, p. 105.
[71] A. Schenck and F. N. Gygax, in *Handbook of Magnetic Materials*, edited by K. H. J. Buschow (Elsevier, Amsterdam, 1995), Vol. 9.
[72] S. F. J. Cox, J. Phys. C **20**, 3187 (1987).
[73] J. L. Dormann, Rev. Phys. Appl. **16**, 275 (1981).
[74] S. Mørup, F. Bødker, P. V. Hendriksen, and S. Linderoth, Phys. Rev. B **52**, 287 (1995).
[75] J. A. de Toro, M. A. López de la Torre, J. M. Riveiro, R. Saez Puche, A. Gómez Herrero, and L. C. Otero Diaz, Phys. Rev. B **60**, 12 918 (1999).
[76] C. Djurberg, P. Svedlindh, P. Nordblad, M. F. Hansen, F. Bødker, and S. Mørup, Phys. Rev. Lett. **79**, 5154 (1997).
[77] T. Kemeny, D. Kaptas, J. Balogh, L. F. Kiss, T. Pusztai, and I. Vincze, J. Phys.: Condens. Matter **11**, 2841 (1999).
[78] G. M. Genkin and M. V. Sapozhnikov, Appl. Phys. Lett. **64**, 794 (1994).
[79] D. Altbir, J. d'Alburquerque e Castro, and P. Vargas, Phys. Rev. B **54**, R6823 (1996).